

Supplementary Information

Prior limits on SN Ia progenitors from optical data

Nine Type Ia supernovae (SNe Ia) with preexisting *Hubble Space Telescope* (*HST*) data on their host galaxies have been close enough (within 25 Mpc) to search for a progenitor (Supplementary Table 1). No progenitor system has been found; only upper limits have been possible^{31,8,9,10}. Limits range from $M_g = -3.9$ mag in the case of SN 2004W to $M_I = -8.3$ mag for SN 2003cg³¹. These limits provided only poor constraints; in the case of SN 2006dd and SN 2006mr in NGC 1316, they ruled out normal stars with initial masses greater than $6 M_\odot$ at the tip of the asymptotic giant branch (AGB), young post-AGB stars with initial masses greater than $4 M_\odot$, and post-red-giant stars with initial masses greater than $9 M_\odot$ ⁸.

HST data reduction

Search for the progenitor system of SN 2011fe

We searched the *HST* data archive and found six datasets that contain the site of SN 2011fe. These include the Advanced Camera for Surveys (ACS) images observed in the F435W, F555W, and F814W filters in program GO-9490 (PI: K. Kuntz) on 2002 Nov. 13, a pair of images observed with the Wide Field Planetary Camera 2 (WFPC2) in the F606W filter in program GO-7909 (PI: S. Casertano) on 1998 May 22, and a Wide Field Camera 3 (WFC3) image observed in the F469N filter in program GO-11635 (PI: M. Shara) on 2010 Apr 8. More details on the available *HST* data are listed in Supplementary Table 2.

To initially locate the site of SN 2011fe in these images, we utilised the PTF discovery images reported by Nugent et al. (2011a)³². We followed the general procedure to identify SN progenitors in high-resolution *HST* images as reported by, for example, Li et al. (2005)³³. We first registered the PTF images to a deep *r*-band MegaCam image downloaded from the 3.6-m Canada-France-Hawaii Telescope (CFHT) science data archive^{1†}. Twelve stars were used in the astrometric solution for this step, yielding a precision of $1\sigma = 0''.055$. The CFHT MegaCam image was further registered to the ACS/F814W image. The astrometric solution, using 16 stars, has a precision of $1\sigma = 0''.017$. The 1σ uncertainty of the final SN location in the ACS/F814W image is $0''.058 = 58$ mas. No object is visible at the nominal position of SN 2011fe in any of the *HST* images. This finding was reported as an astronomer's telegram (ATEL; Li et al. 2011a)³⁴. We noted in our ATEL the presence of two red sources within roughly the $2 \times 1\sigma$ uncertainty of our solution. Further analysis of these two sources was reported by Li et al. (2011b)³⁵.

To improve our astrometric solution, on 2011 August 26 we observed the field of SN 2011fe with the Near-Infrared Camera 2 (NIRC2) mounted behind the adaptive optics (AO) system on the Keck II telescope¹⁵. Beginning at 5:33 UT, we obtained a series of *H*-band exposures, each consisting of 30 nondestructive readouts of 2 s each, for a total time on source of 360 s. The SN was sufficiently bright to use as the guide star for the tip-tilt correction. Images were reduced using standard IRAF^{2†} routines, using a median combination of the (nonaligned) dithered images to correct for the sky background. Prior to registration, we applied the distortion correction provided by the Keck Observatory^{3†}. The dithered images were registered and stacked to produce a single image with a resolution of $0''.04 \text{ pixel}^{-1}$, slightly superior to the resolution of the ACS images ($0''.05 \text{ pixel}^{-1}$).

We were able to identify 13 stars around the SN position that are present in both the Keck AO and ACS/F814W images (Supplementary Figure 1). The astrometric solution of this set of objects is limited by the difficulties of accurately measuring the centroid positions for the stars on the Keck AO images due to the low signal-to-noise ratios (S/N) of the detections. Nonetheless, the solution has a precision of $1\sigma = 0''.021$ or 21 mas, much improved over our reported precision (58 mas) in Li et al. (2011a)³⁴. The SN location in the ACS/F814W image (filename: HST_9490_a2_ACS_WFC_F814W_sci.fits) is $X = 3309.30$, $Y = 1750.12$, with an uncertainty of 0.30 pixel in both axes. This position is consistent with our preliminary analysis³⁴ to within 1σ uncertainty, and also agrees with the

^{1†} This research used the facilities of the Canadian Astronomy Data Centre operated by the National Research Council of Canada with the support of the Canadian Space Agency.

^{2†} IRAF is distributed by the National Optical Astronomy Observatory, which is operated by the Association of Universities for Research in Astronomy (AURA), Inc., under cooperative agreement with the US National Science Foundation (NSF).

^{3†} See http://www2.keck.hawaii.edu/inst/nirc2/forReDoc/post_observing/dewarp.

Supernova	Distance (Mpc)		Limits (mag) ^a	Reference
SN 2003cg	17.3	$M_R = -7.1$	$M_I = -8.3$	31
SN 2003gs	17.9	$M_V = -6.2$		31
SN 2003hv	21.3	$M_V = -6.3$	$M_I = -6.8$	31
SN 2004W	17.3	$M_g = -3.9$	$M_Z = -5.5$	31
SN 2005df	24	$M_B = -6.2$	$M_R = -5.1$	31
SN 2006dd ^b	19	$M_{B*} = -5.4$	$M_V = -5.3$ $M_I = -6.0$	8
SN 2006mr ^b	19	$M_{B*} = -5.6$	$M_V = -5.4$ $M_I = -6.0$	8
SN 2007sr	12–25	$M_V = -5.5$ to -4.1	$M_I = -7.5$ to -5.6	9
SN 2007on	20	$M_g = -4.5$	$M_I = -4.5$	10

Supplementary Table 1 — Limits on SN Ia progenitors from preexisting *HST* data.

^aFilter Key: $B = F450W$, $B^* = F435W$, $g = F475W$, $V = 555W$, $R = F606W$, $I = F814W$, $Z = F850LP$. Photometric system is AB for ref. 8, Vega for ref. 10. Others are not stated.

^bBoth SN 2006dd and SN 2006mr were located in the same galaxy, NGC 1316.

Dataset	Date(obs)	Exptime(s)	Instrument	Aperture	Filter	Prop. No.	Label ^a
J8D6A2011	2002-11-13	900.0	ACS	WFC	F435W	9490	ACS/F435W
J8D6A2021	2002-11-13	720.0	ACS	WFC	F555W	9490	ACS/F555W
J8D6A2031	2002-11-13	720.0	ACS	WFC	F814W	9490	ACS/F814W
U4K2KF02R	1998-05-22	260.0	WFPC2	WFALL	F606W	7909	WFPC2/F606W
U4K2KF01R	1998-05-22	260.0	WFPC2	WFALL	F606W	7909	WFPC2/F606W
IB3P17010	2010-04-08	6106.0	WFC3	UVIS	F469N	11635	WFC3/F469N

Supplementary Table 2 — Available *HST* data at the location of SN 2011fe.

^aThese labels are used in the text to represent the images.

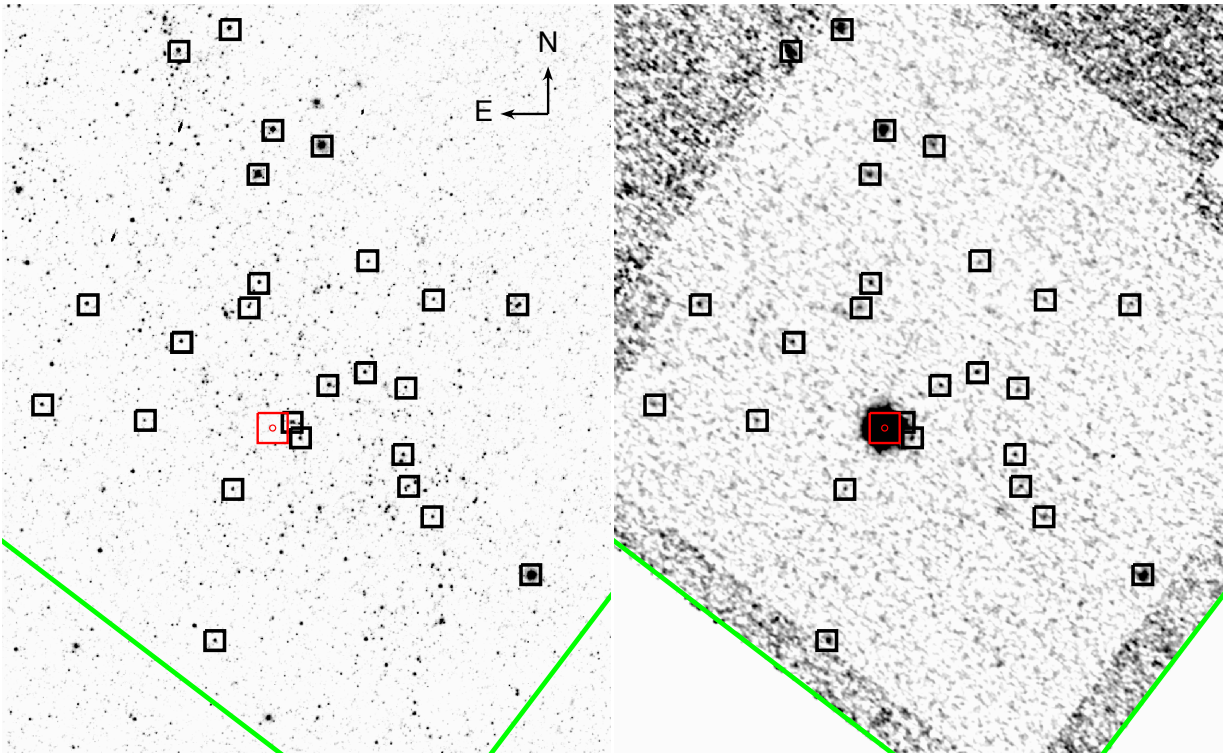
position reported by Smartt et al. (2011)³⁶. The precise position for the SN location is $\alpha = 14^h03^m05^s.733$, $\delta = +54^\circ16'25''.18$ (J2000.0) in the world coordinate system (WCS) of the ACS/F814W image.

The site of SN 2011fe in the other *HST* data reported in Supplementary Table 2 was carefully inspected, and no object was detected in any of the images. In the next section, we derive the limiting magnitudes of the *HST* data.

Limiting magnitudes

We employed several methods to derive limiting magnitudes for the *HST* images. For method I, the photometry for many stars near the SN position was measured, and the measured magnitude that gives an error of 0.2 mag is considered to be the 5σ upper limit. The 3σ upper limit is then 0.4 mag deeper. To perform photometry of the stars, we have followed the recipes described by Sirianni et al. (2005)³⁷ for ACS and by Holtzman et al. (1995a, 1995b)^{38,39} for WFPC2. For method II, we measured the variance of the sky background in the immediate vicinity of the SN. This variance, along with the instrument characteristics, was used to calculate the brightness for objects with different S/N. For method III, we made use of the Exposure Time Calculator (ETC) available from STScI. Assuming a flat continuum in F_λ , we derived the magnitude for an object that would be detected at different S/N with the setup of the *HST* observations. The three methods yield limiting magnitudes that are in general within 0.1 mag of each other, and their average values are reported in Supplementary Table 3.

While the limiting magnitudes of the individual *HST* datasets already reach great depth, the ensemble of all the *HST* data, when considered together, offers even greater depth. We focus this analysis on the V band. Since the *HST*



Supplementary Figure 1 — Astrometric solution using the Keck AO image. The Keck AO image is shown in the right panel, and is astrometrically matched to a section of *HST* ACS/F814W image on the left panel. The field of view is $1' \times 1'$. Detected objects in the Keck AO images (and the counterparts in the *HST* image) are marked with black squares. Thirteen with the largest S/N and with reasonably accurate positions are used in the astrometric solution, achieving a 1σ precision of 21 mas. The red square is centred on the SN and has a scale of $2'' \times 2''$, matching the scale of the right panel presented in Figure 1 of the main text. The green lines mark the boundary of the AO image in the ACS/F814W image.

Label	3.0σ	2.5σ	2.0σ
ACS/F435W	27.42	27.62	27.87
ACS/F555W	27.04	27.25	27.49
ACS/F814W	26.35	26.55	26.81
WFPC2/F606W	26.60	26.80	27.05

Supplementary Table 3 — Limiting magnitudes of the *HST* images in the Vega magnitude system.

data were observed with different filters, they can only be combined if the spectral type of the object of interest is known. We have made use of the spectrum database for the different spectral types published by Castelli & Kurucz (2004)⁴⁰, augmented with blackbody spectra for extremely hot stars, and Pickles (1998)⁴¹ spectra of very cool stars and brown dwarfs.

For each spectral type, we first derived the tightest limiting magnitude for the *V* band from the 4 individual *HST* images. Using the “synphot” package in IRAF/STSDAS, we converted the limiting magnitudes derived for the ACS/F435W (*B* band) and ACS/F814W (*I* band) into effective limiting magnitudes in the *V* band. The deepest *V*-band magnitude among the 4 measurements is then chosen as our “1-frame” limiting magnitude in the *V* band. Not surprisingly, when the spectral type is blue (such as O and B stars), the *HST* data observed with the blue filter (ACS/F435W) provide the deepest *V*-band limit, while for the red spectral types (K and M stars), the *HST* data in ACS/F814W are the deepest.

We then derived the limiting magnitude for the stacked *HST* data. We employed two methods to do this. For method “a” (“time-stacked” method, hereafter), we converted the *HST* data observed with ACS/F435W, ACS/F814W, and WFPC2/F606W into “effective” ACS/F555W observations. We discuss ACS/F435W as an example. For a given spectral type, the *B*-band limiting magnitude was converted to the *V* band using synphot. Using ETC, we derived the “effective” exposure time at which ACS/F555W would reach the same *V*-band limiting magnitude (for the said spectral type). The stacked *HST* data were then considered as an ACS/F555W observation with an exposure time that is the sum of all the “effective” exposure times, and the limiting magnitudes were derived using ETC. In general, the limiting magnitude for the stacked image is deeper than the “1-frame” limits by 0.2–0.8 mag.

We also used an alternate method “b” (“flux-stacked” method, hereafter) to determine an effective limiting *V* magnitude from “stacking” the *HST* images. We began with the same synphot calculated colours for the full range of spectral types used above. We then calculated the χ^2 goodness-of-fit statistic for each spectral type, varying the *V* magnitude over a wide range, and comparing the model flux with the measurements. The calculation was performed in flux units, with the uncertainty in the measured flux derived from observed 3σ upper limits given in Supplementary Table 3. We then tabulated 2σ , 2.5σ , and 3σ effective limits to the *V* magnitude by determining where the fit probability reaches 0.9545, 0.9876, and 0.9973, respectively. The method is illustrated in Supplementary Figure 2, which shows the calculation for a K0 III model. Our results with this method were similar to those using the effective exposure time method above, and so we have averaged the two in determining our final constraints.

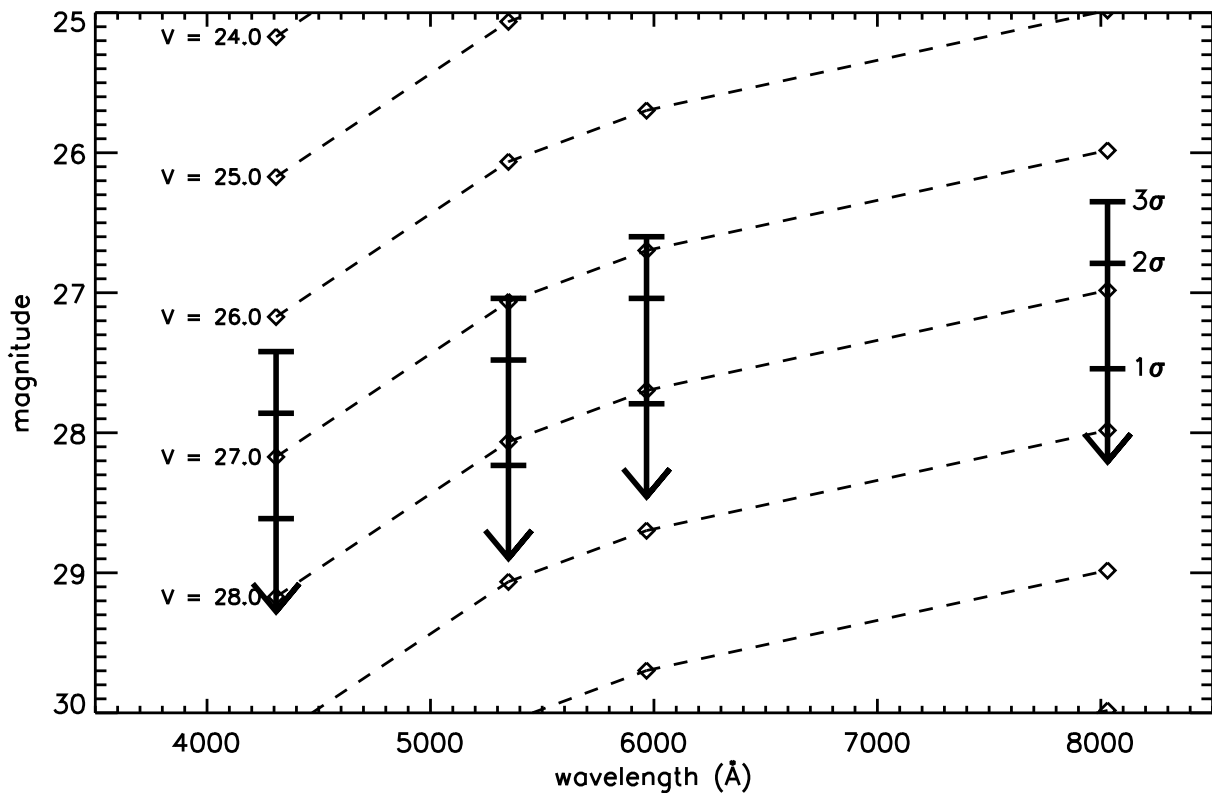
The reddening toward SN 2011fe is negligible in the Galaxy [$E(B - V) = 0.009$ mag]⁴² and in M101 (Nugent et al. 2011b). Adopting a distance modulus of $\mu = 29.05 \pm 0.23$ mag^{27,28}, the *V*-band magnitude limits in Supplementary Table 3 can be converted to absolute magnitudes $M(V)$. We fit a cubic spline function to the 2σ limiting magnitudes as a function of the effective temperatures of the different spectral types, and present the results in a Hertzsprung-Russell diagram (H-R diagram, Figure 2 of the main text).

Implications on the progenitor system of SN 2011fe from the H-R diagram

SNe Ia are believed to be caused by the thermonuclear explosion of a WD composed mainly of carbon and oxygen (i.e., a CO WD). In the most popular models, this is due to the degenerate ignition of carbon when the mass of the CO WD approaches the Chandrasekhar mass ($\sim 1.4 M_{\odot}$), the maximum possible mass for a WD^{4†}.

One of the main unsolved questions is what makes a WD grow to the Chandrasekhar mass. To summarise what was presented in the main text, there are numerous progenitor models which broadly follow into two classes: *double-degenerate (DD) models*^{2,4} and *single-degenerate (SD) models*^{1,3}. In the DD models, two CO white dwarfs in a close binary are driven together by the emission of gravitational waves until the lighter WD is disrupted dynamically, leading to the merger of the two. A SN Ia may occur when the combined mass approaches the Chandrasekhar mass. In the SD models, the mass of the CO white dwarfs grows by accretion of matter from a companion star. Different SD models can be distinguished based on the nature of the mass donor: this can be either a main-sequence star or subgiant (“super-soft channel”¹²), a giant star (“symbiotic channel”¹¹), a helium star (“helium-star channel”^{1,13,14}), or perhaps even a degenerate object.

^{4†} There are also alternative models in which the exploding WD is below the Chandrasekhar mass, so-called sub-Chandrasekhar models. In these models, carbon may be ignited by a detonation wave caused by the detonation of helium in a shell surrounding the CO core (i.e., “double-detonation models”^{43,44}).



Supplementary Figure 2 — Illustration of the χ^2 method to determine the effective limiting V magnitude from “stacking” the *HST* observations. The thick arrows show the observed upper limits in ACS/F435W, ACS/F555W, WFPC2/F606W, and ACS/F814W from left to right (all in the VEGAMAG system), and are hatched at 3σ , 2σ , and 1σ (in flux units) from top to bottom. The open diamonds (connected by dashed lines) show the synphot-calculated magnitudes for a K0 III star over a range of V brightnesses. We calculated the χ^2 statistic as a function of V magnitude to determine the effective V magnitude limits from all the data combined. In this example we find $V > 28.19$, 27.95 , and 27.75 mag at 2σ , 2.5σ , and 3σ , respectively.

Sp. Type	3.0 σ		2.5 σ		2.0 σ	
	"1"-frame	stacked	"1"-frame	stacked	"1"-frame	stacked
O3 V	27.74	28.02	27.94	28.22	28.19	28.47
O5 V	27.74	28.03	27.94	28.23	28.19	28.48
B0 V	27.70	28.00	27.90	28.20	28.15	28.45
B5 V	27.58	27.93	27.78	28.13	28.03	28.38
A0 V	27.44	27.86	27.64	28.06	27.89	28.31
A5 V	27.31	27.82	27.51	28.02	27.76	28.27
F0 V	27.15	27.78	27.35	27.98	27.60	28.23
F5 V	27.10	27.78	27.30	27.98	27.55	28.23
G0 V	27.10	27.78	27.30	27.98	27.55	28.23
G5 V	27.10	27.78	27.30	27.98	27.55	28.23
K0 V	27.21	27.81	27.41	28.01	27.66	28.26
K5 V	27.77	28.05	27.97	28.25	28.22	28.50
M0 V	28.31	28.41	28.51	28.61	28.76	28.86
M4 V ^a	—	29.25	—	29.45	—	29.70
M5 V ^a	—	29.61	—	29.81	—	30.06
B0 III	27.69	28.00	27.89	28.20	28.14	28.45
B5 III	27.59	27.93	27.79	28.13	28.04	28.38
G0 III	27.10	27.78	27.30	27.98	27.55	28.23
G5 III	27.20	27.80	27.40	28.00	27.65	28.25
K0 III	27.39	27.86	27.59	28.06	27.84	28.31
K5 III	27.89	28.12	28.09	28.32	28.34	28.57
M0 III	28.25	28.36	28.45	28.56	28.70	28.81
M5 III ^a	—	29.28	—	29.48	—	29.73
M10 III ^a	—	30.89	—	31.09	—	31.34
BO I	27.67	27.98	27.87	28.18	28.12	28.43
B5 I	27.57	27.93	27.77	28.13	28.02	28.38
AO I	27.48	27.89	27.68	28.09	27.93	28.34
A5 I	27.44	27.87	27.64	28.07	27.89	28.32
F0 I	27.36	27.84	27.56	28.04	27.81	28.29
F5 I	27.23	27.81	27.43	28.01	27.68	28.26
G0 I	27.11	27.78	27.31	27.98	27.56	28.23
G5 I	27.40	27.85	27.60	28.05	27.85	28.30
K0 I	27.51	27.90	27.71	28.10	27.96	28.35
K5 I	28.20	28.32	28.40	28.52	28.65	28.77
M0 I	28.19	28.32	28.39	28.52	28.64	28.77
M2 I	28.77	28.78	28.97	28.98	29.22	29.23
BB1 ^b	—	27.91	—	28.11	—	28.36
BB2 ^b	—	27.94	—	28.14	—	28.39
BB3 ^b	—	27.96	—	28.16	—	28.41

Supplementary Table 4 — Limiting magnitudes in the V band for the “stacked” *HST* image.

^aFor these spectral types, the spectra from Pickles (1998)⁴¹ were used, and only the “flux-stacked” limits were derived.

^bBlackbody spectra with $T_{\text{eff}} = 35,000$ K (BB1), 60,000 K (BB2), and 100,000 K (BB3). For these spectra, only the “flux-stacked” limits were derived.

All of these proposed models have their advantages and problems, and there are numerous observational constraints ruling out particular models in individual cases; see, for example, Podsiadlowski et al. (2008)⁶ for further discussion. In addition, it is quite possible, perhaps even likely, that more than one progenitor channel is required to explain the observed diversity among SNe Ia.

Because it is relatively nearby, SN 2011fe provides a unique opportunity to constrain the various proposed progenitor models, at least for this SN. Figure 2 in the main text shows the upper M_V limits in an H-R diagram from deep pre-SN *HST* images. The figure also indicates the location of various observed systems in our Galaxy that have been suggested to be prototypical SN Ia progenitor systems in the SD channel: RS Oph and T CrB are symbiotic binaries with orbital periods of 455 and 228 days, respectively, representing the symbiotic channel¹⁶; U Sco is a supersoft source with an orbital period of 30 hr¹⁸; and V445 Pup is a binary with a helium-star donor which underwent a helium nova in 2000 (its orbital period has not yet been determined)^{45,17}. In all of these systems, the WDs are believed to have a mass close to the Chandrasekhar mass, making them excellent candidates for SN Ia progenitors^{5†}.

As Figure 2 shows, the *HST* images already constrain possible progenitor models. In particular, the data strongly argue against a symbiotic binary progenitor, ruling out a system like RS Oph and probably T CrB. Similarly, a helium-star binary such as V445 Pup is not consistent with the upper limits, although He-star donors cannot be completely ruled out (see the blue-shaded area labelled “He-star channel” in Figure 1). Among the SD models, only the supersoft channel can easily be reconciled with the *HST* constraints. Finally, all DD models are consistent with the nondetection of a source at the position of SN 2011fe, as it does not predict a bright source in the visible range.

There are a few caveats on the constraints on the symbiotic channel. The circumstellar matter (CSM) is likely to be aspherically distributed around the binary progenitor system in a symbiotic channel; consequently, the extinction due to CSM depends on the inclination of the binary orbit and the observer’s viewing angle. A luminous red-giant companion star thus could elude detection if it suffers a large amount of extinction due to CSM. Also, according to a recently proposed spin-down scenario^{46,47}, the CO WD may have to spin down before it can explode. In this case, if the required spin-down time is sufficiently long, a red-giant companion in a symbiotic system could have evolved into a helium WD. Such a helium WD companion in the symbiotic binary channel could not be ruled out for SN 2011fe.

The tip of the red-giant branch (TRGB) is defined as a sharp cutoff of the luminosity function of the brightest red-giant-branch stars in a galaxy, and is an important distance indicator^{48,49}. The luminosity function is generally derived in the *I* band, where the magnitude of the TRGB stars is insensitive to metallicity and age of the stellar population. For $T_{\text{eff}} \approx 3000\text{--}4000$ K, as expected for the red-giant branch (RGB) stars, the M_V limit we derived at the site of SN 2011fe excludes stars brighter than an absolute *I*-band mag $M_I \approx -2$. This limit is 2 mag fainter than the observed²⁸ TRGB in M101. Both “star 1” and “star 2” marked in Figure 1 of the main text, on the other hand, were measured to have $M_I \approx -4$ mag and $V - I$ colors of 1.8 mag and redder³⁵, and are thus consistent with being TRGB stars.

For a given effective temperature and M_V limit the minimum effective radius $R_{\text{eff,min}}$ of the allowed progenitor can be calculated assuming a “bolometric correction” from the *V* band to the total bolometric luminosity $[BC_V(T_{\text{eff}})]$ ³⁰. At $T_{\text{eff}} = 3000$ K, $BC_V = -5.00$ mag; at $T_{\text{eff}} = 4000$ K, $BC_V = -1.12$ mag. We take $R_{\text{eff,min}}$ to be

$$R_{\text{eff,min}}/R_{\odot} = \frac{10^{8.4694 - 0.2[BC_V(T_{\text{eff}}) + M_V]}}{T_{\text{eff}}^2},$$

where M_V is the limit we calculate above. At $T_{\text{eff}} = 3010, 3490$, and 4050 K we find (respectively) limits of $M_V = 0.59, 0.24$, and -0.22 mag, and $R_{\text{eff,min}} = 240, 63$, and $32 R_{\odot}$ (with R_{\odot} being the radius of the Sun).

In summary, the progenitor models that are most consistent with the historical constraint are either the supersoft SD channel or any DD model.

Notes on the constraints from observed SN Ia progenitor candidates

Figure 2 in the main text indicates the location in the H-R diagram of some suggested SN Ia candidate progenitor systems in the Milky Way. For these systems we plot the effective temperature based on estimates of the spectral type (if available) or theoretical modelling of the donor star. The absolute magnitudes are taken from observations of these systems in quiescence and include, in addition to the light from the donor star, the contributions from the hot

^{5†} As a caveat, it should be noted that it is not established in any of these systems whether the WD is a CO white dwarf or an ONeMg white dwarf. In the latter case, the WD would not undergo a thermonuclear explosion when it reaches the Chandrasekhar mass, but rather experience collapse to a neutron star, not producing a SN Ia.

accreting WD and the accretion disk, which may be quite substantial. The large uncertainties in the inferred absolute magnitudes are mostly due to uncertainties in the distance estimates and the applicable extinctions.

RS Oph and T CrB

RS Oph and T CrB are symbiotic binaries where the WD is close to the Chandrasekhar mass and experiences recurrent novae. RS Oph during quiescence has m_V varying between ~ 11 and ~ 11.5 mag⁵⁰. Recent distance estimates range from 1.4 kpc (from modelling of the last outburst) to 3.1 kpc (assuming the secondary is filling its Roche lobe; see Barry et al. (2008)⁵¹ for discussion). Using an estimate of the visual extinction of 2 mag (Iijima 2008)⁵² then leads to an estimated range of M_V from -1.2 to -3.5 . The spectral type of the donor has been determined to be M0 to M2 III (Anupama & Mikołajewska 1999)⁵³, implying an effective temperature of 3750 to 3900 K (Straizys & Kuriliene 1981)⁵⁴.

T CrB has a quiescent $m_V \approx 10$ mag. With a distance estimate in the range of 0.9 to 1.3 kpc and an adopted extinction of ~ 0.5 mag (Belczynski & Mikołajewska 1998)⁵⁵, this leads to an absolute M_V of -1 to $+0$ mag. Its estimated spectral type of M3/4 III implies an effective temperature for the donor of 3550 to 3650 K (Straizys & Kuriliene 1981)⁵⁴.

U Sco

U Sco is supersoft recurrent nova with a very massive WD. Since its distance is not well established, we plot typical parameters for a system of this type from the modelling by Podsiadlowski (2003)^{56†}. Adopting a reasonable range in properties leads to a range in M_V of 2.5 to 3.9 mag and a range of T_{eff} of 5200 to 6000 K.

V 445 Pup

V 445 Pup experienced a helium nova in 2000 and is a prototypical system for a SD model with a helium-star donor. Woudt et al. (2009)¹⁷ have determined the distance from an expansion parallax to be 8.2 ± 0.5 kpc. The extinction is highly uncertain and may contain contributions both from the interstellar medium and the CSM, leading to a large uncertainty in the dereddened M_V from -1.7 to -4.5 (Woudt et al. 2009). Even the lower limit seems firmly ruled out by our pre-supernova constraints, unless there is much CSM extinction in the orbital plane and the system is viewed along this plane. The effective temperature of the donor star is not well determined, but the helium stellar models of Liu et al. (2010)¹³ suggest a temperature between 50,000 K and 100,000 K for a system like V 445 Pup. We plot the estimated M_V range for V 445 Pup near the theoretical models for the He-star channel¹³.

He-star channel

For the He-star channel we adopt the theoretical models of Liu et al. (2010)¹³, taking the properties of the donor star at the time of explosion (their Fig. 6) and applying appropriate bolometric corrections from Torres (2010)³⁰.

Historical light curves

RS Oph, T CrB, and U Sco are recurrent novae. Indeed, the recurrence time of WD binaries where the WD is close to the Chandrasekhar mass is expected to be 10–20 yr¹⁹. Regular ground-based optical imaging of M101 has been obtained with four facilities during the course of the past ~ 13 years: the 0.76-m Katzman Automatic Imaging Telescope (KAIT) on Mount Hamilton, CA, as part of the Lick Observatory Supernova Search (LOSS;⁵⁷); the Palomar 60-in telescope (P60;⁵⁸) as part of the P60 Fast Transients in Nearest Galaxies survey (FastTING;⁵⁹); the 3.6-m Canada-France-Hawaii Telescope on Mauna Kea; and the Palomar 48-in as part of the ongoing Palomar Transient Factory^{60,61}. In addition to the ground-based imaging, M101 was observed multiple times by *HST*; see the discussion in the previous section of the supplementary material. All of the ground-based images were reduced using standard techniques, including removal of the bias and dark current from each frame followed by proper flatfielding.

The projected position of SN 2011fe lies very close to a spiral arm structure within M101, leading to a complex background region in the vicinity of the SN (see Figure 1 of the main text). Thus, in order to search for any variable optical emission that may be associated with the progenitor system of SN 2011fe, we employed image subtraction to remove the complex, but presumably static, background signal. For each individual image (hereafter, new image), a reference image was constructed using a deep coaddition of several images taken with the same camera and in the same filter but during a different year than the new image to ensure that any possible variable emission in the new

^{6†} These parameters are typical for progenitors in the supersoft channel, regardless of whether the WD in U Sco is a CO or ONeMg WD.

frames is not also present in the reference image. Following the construction of appropriate reference images, for each new image the corresponding reference was then astrometrically aligned with the new image, both images were convolved to have the same seeing, and the flux in the reference image was then subtracted from the flux in the new image.

Following proper subtraction, we examined whether any variable emission can be detected at the location of the SN. We measured the flux in an aperture centred on the SN position, which is precisely measured to an accuracy < 1 pixel by transforming a P48 image that contains the SN to the same coordinates as the subtracted image. To determine the uncertainty in this single-aperture measurement, we measured the variance in 1000 apertures randomly placed within a $\sim 90'' \times 90''$ box centred on the SN position, which ensures similar background properties as the SN position but excludes strong systematic variations related to residuals associated with poorly subtracted bright stars. Using this method there are multiple images where we detect flux at the SN position with greater than 3σ confidence; however, since we have ~ 3000 images of M101, we would expect about five 3σ detections based on Gaussian fluctuations. In order to test the null hypothesis that no emission is present in the subtraction images, with the alternative hypothesis that emission is present in an image, we employ the false-discovery rate method (FDR; see Benjamin & Hochberg (1995)⁶², Miller et al. (2001)⁶³) which controls for the fact that in multiple-hypothesis testing, in this case many images, there are multiple comparisons to the null hypothesis. Using the FDR method, and setting $\alpha = 0.05$ (equivalent to a 2σ detection), we are unable to reject the null hypothesis that no variable emission is present at the position of the SN. This result is not surprising given that the typical individual images from KAIT [$m_{\text{clear}}(3\sigma) \approx 18.8$ mag], P48 [$m_{\text{Mould-R}}(3\sigma) \approx 21$ mag], and P60 [$m_g(3\sigma) \approx 21.5$ mag] are too shallow to detect all but the very brightest novae (see Figure 3), and even that would require an image to be taken within a few days of the peak brightness of the nova. While the CFHT images are deep enough to detect even the very faintest novae, since only 7 images were taken over slightly more than 7 yr the probability of a nova being bright enough for detection concurrently with an acquired image is only $\sim 7\%$.

To further constrain the possibility of pre-SN variability, we stack individual images grouped closely together in time in order to obtain limits that are deeper than those in the individual frames. Should variable emission, such as that associated with a nova, be present within the data, then the stacked images will reflect the average observed flux from each of the individual images. On week-to-month timescales the detection threshold for stacked images decreases *faster* than the average flux from a nova, and therefore stacked images will allow an improved opportunity for the detection of variability on timescales similar to those of a nova. For KAIT we stacked images on intervals of 30 days and for entire observing seasons. These images extend over the full lifetime of LOSS, ~ 13 yr, and are shown in black in Figure 3. For the P60 we employ both 7 day and 30 day stacks which extend from late 2006 through mid 2009, shown in green in Figure 3. For the P48 observations of M101 we employ 7 day and 30 day stacks extending over the full lifetime of PTF from mid-2009 to the present. These limits are shown in red in Figure 3. Following the production of stacked images, we use the same procedure described above to test for variable emission: we subtract the flux from a template image and measure the flux at the SN position compared with several randomly placed apertures in the vicinity of the SN position. Using the FDR method, we once again find no significant detection of variable emission at the position of the SN.

Following the nondetection of any pre-SN variability, we attempt to constrain the probability that a nova could have occurred in the 13 yr prior to SN 2011fe but that gaps in our observations or insufficient depth in our stacked images prevented us from detecting the signal. The true characterisation of this probability requires an *a priori* knowledge of the nova luminosity function (NLF) including the distribution of nova rise times, which are typically short; see, e.g., Kasliwal et al. (2011)⁵⁹. To the best of our knowledge, a complete sample of the distribution of the NLF has not been assembled to date, and thus we must use proxies in our estimates of the probability of detecting a nova signal. As a proxy for the true NLF we use the light curves of two novae discovered during the FasTING survey in M31, nova 2008-09a and nova 2008-09c⁵⁹. We elect to use extragalactic novae to avoid the large systematic uncertainties associated with measuring the distance and reddening toward Galactic novae, and in particular, the two selected novae have strong constraints on the rise time as a result of the high-cadence observations from FasTING. We can characterise these two novae using the maximum-magnitude vs. rate-of-decline (MMRD) relation (for a theoretical explanation see, e.g., Livio (1992)⁶⁴, although see also Kasliwal et al. (2011)⁵⁹), from which we learn that nova 2008-09c is a typical nova with $M_g = -7.8$ mag and a time to decline from peak by 1 mag, $t_1 = 9.1$ days⁵⁹. Nova 2008-09a, on the other hand, is both faint, $M_g = -6.8$ mag, and fast evolving, $t_1 = 6.3$ days⁵⁹, meaning it is among the most challenging type of nova

to detect. Using a smooth spline fit to the data for these two novae, we deredden them and shift them to the distance of M101 to serve as a proxy to the true NLF. The light curves for each of these novae are shown in Figure 3: 2008-09c is in green, while 2008-09a is in blue.

The typical detection limits from KAIT are too shallow to detect all but the most luminous novae, and even in these cases the signal would often be degraded given the large number of KAIT images needed to reach a detection threshold of $m > 21.5$ mag. Therefore, we focus our efforts on constraining the presence of a nova during the time of the P60 and PTF observations, which constrains the following limits to the past five observing seasons starting from late 2006 until the time of the SN (see the bottom panel of Figure 3). To determine the detection probabilities, at random times we insert a fake nova signal into the data and determine the average flux from the nova based on the actual observation times of the stacked images that overlap the nova in time. If the average flux is greater than the measured detection threshold from the stacked image, then the nova is considered detected. We have repeated this procedure 1 million times for each of our example novae, and we find a detection probability of 2008-09a-like and 2008-09c-like novae of 0.440 and 0.628, respectively.

It is important to note, however, that these detection limits provide a *lower limit* to the true detection probability since we have adopted a stacking scheme that does not include overlapping windows (the precise scheme we use can be visualised using the horizontal error bars of the limits shown in Figure 3). Under this method a nova that peaks directly in between two stacking windows could escape detection, as each window overlaps with only a fraction of the nova. To prevent this from happening, an additional window, preferably centred near the time of peak brightness from the nova, should be created. Given the broad complexities associated with the image sequences, for example variable cadence and detection thresholds, the ideal method to test for the presence of a nova would be to stack all the images in every possible grouping on timescales shorter than those typical for a nova, ~ 30 days. Such an effort would be impractical for the ~ 3000 pre-SN images of M101 discussed here, and is beyond the scope of the current paper.

X-ray upper limits

We analysed 11 epochs of *Chandra* observations of the field containing SN 2011fe, all taken in 2004. Additional observations in which the SN location is near one of the CCD edges were removed. We detected no bright source in any epochs, and we additionally subselected the epochs capable of producing the most stringent flux limit. These were the 4 epochs (ObsIDs 6114, 6115, 4735, and 6118) where the SN was within $3.5'$ of the observation aimpoint, placing the source on the most sensitive ACIS-S3 detector. The total exposure in these 4 epochs is 142 ks.

Count rates and spectra were extracted from a 4-pixel ($2''$) radius aperture, containing 90% of the encircled photon flux, around the SN position for each epoch using standard tools in CIAO 4.3^{7†}. The sky background was estimated using an annular extraction region with an inner radius of 20 pixels and an outer radius of 50 pixels about the source position. Given 9 counts (0.3–8 keV) detected in the source region over an expected background of 11.2 counts, we determine a 3σ upper limit on the source count rate of 9.1×10^{-5} count s^{-1} .

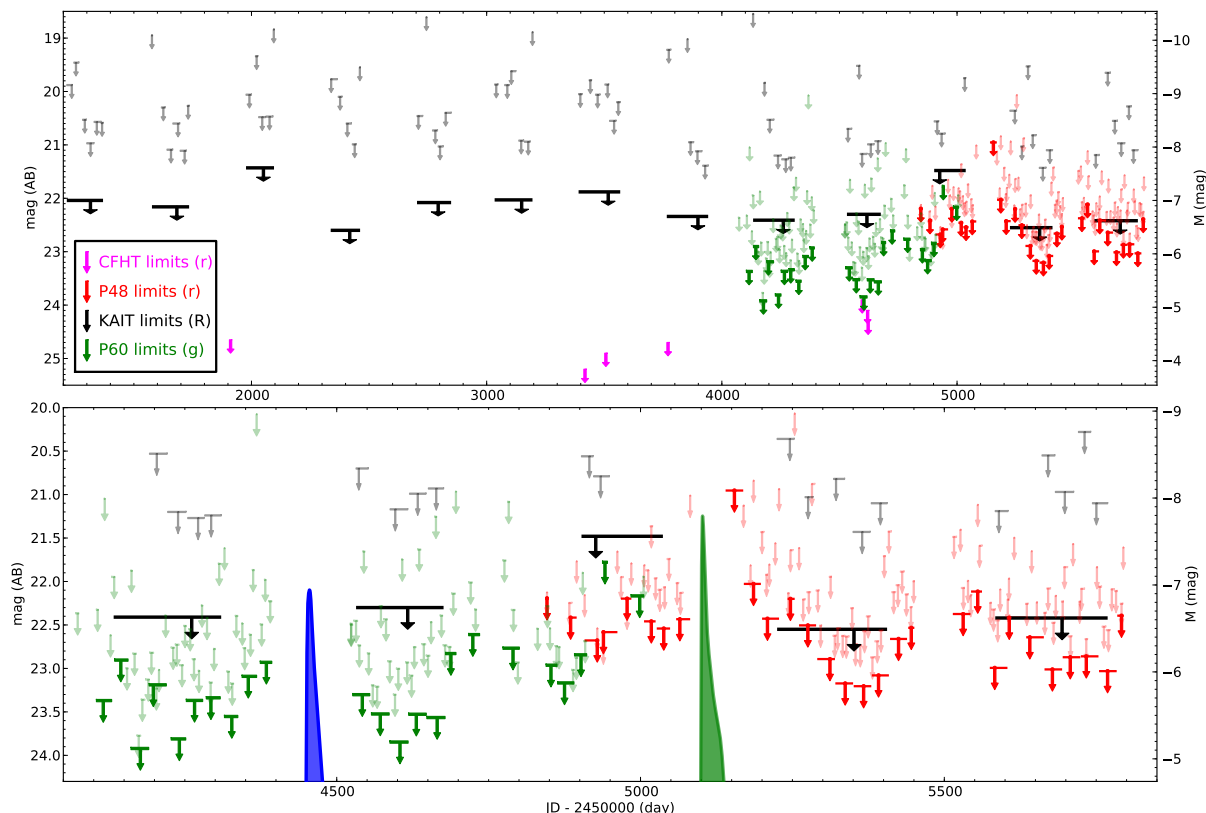
We fit the summed spectra in ISIS^{8†} by minimizing the Cash (1979) statistic⁶⁵. Assuming an absorbed power-law model with photon index $\Gamma = 2$ and Galactic column density⁶⁶ $N_H = 1.8 \times 10^{20} \text{ cm}^{-2}$, we determine a 3σ limiting unabsorbed luminosity of $4.1 \times 10^{36} \text{ erg s}^{-1}$ (0.3–8 keV). For a 67 eV blackbody (e.g., Gilfanov & Bogdan (2011)⁶⁷; see, however, Hachisu et al. (2010)⁶⁸), the bolometric luminosity limit is $2.5 \times 10^{37} \text{ erg s}^{-1}$. Supplementary Figure 4 displays the limit on the progenitor radius as a function of temperature, assuming a blackbody model.

Spitzer data reduction

We analysed preexplosion *Spitzer*/IRAC data taken on UT 2004 March 8.09 and 2004 March 8.49 (PID:60, PI: G. Rieke). Using 12 stars on the PTF discovery images³² that are also present in the *Spitzer* images, we were able to locate the SN position with a 1σ uncertainty of $0''.132$ (132 mas). No point source was detected in any of the *Spitzer* data. Limiting magnitudes were derived in a 20×20 pixel box centred on the location of SN 2011fe; see Supplementary Table 5.

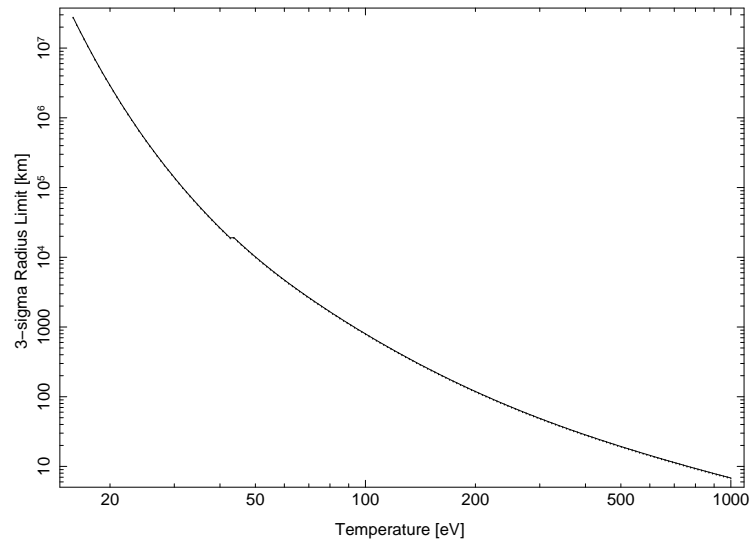
^{7†} <http://cxc.harvard.edu/ciao/index.html>.

^{8†} <http://space.mit.edu/CXC/ISIS>.



Supplementary Figure 3 — Historical limits on pre-SN emission from the progenitor system of SN 2011fe.

Shown in the top panel are the limiting magnitudes for stacked images from pre-SN imaging of M101 from KAIT (R band), CFHT (R/r band), P60 (g band), and PTF (R_{Mould}) extending > 12 yr prior to the SN explosion. The KAIT data are stacked on both monthly (light black) and yearly (dark black) intervals, CFHT limits are shown in magenta, P60 data are stacked on both weekly (light green) and monthly (dark green) intervals, and the PTF/P48 data are stacked on weekly (light red) and monthly (dark red) intervals. The width of the error bars indicates the time elapsed between the first image and the last image included in a stack. The bottom panel shows in detail the ~ 5 yr prior to the SN, when the P60 and P48 data provide the strongest constraints on a possible nova. Overplotted on the data are the light curves of two novae from M31: 2008-09a, a quickly fading, faint nova (blue), and 2008-09c, a typical classical nova (green;⁵⁹), with their apparent brightness scaled to how they would appear in M101. The limits show that we would have been capable of detecting such outbursts, with the probability of detection $\sim 44\%$ and $\sim 63\%$ for 2008-09a-like novae and 2008-09c-like novae, respectively.



Supplementary Figure 4 — The limit on the progenitor radius as a function of temperature assuming a blackbody model, derived from the X-ray luminosity limits.

MJD	Filter (μm)	Absolute Mag Limit (Vega)	νF_ν Limit ($10^{36} \text{ erg s}^{-1}$)
53072.090	3.6	−10.6	1.4
53072.490	3.6	−10.6	1.2
53072.090	4.5	−11.2	1.2
53072.490	4.5	−11.1	1.0
53072.090	5.8	−13.1	11
53072.490	5.8	−13.1	13
53072.090	8.0	−13.8	6.7
53072.490	8.0	−13.9	8.6

Supplementary Table 5 — *Spitzer* 3σ upper limits.

According to a mid-infrared (IR) H-R diagram presented by Ardila et al. (2010)⁶⁹, the mid-IR luminosities for red giants (K0 III to M6 III) are in the range of 4×10^{35} to 4×10^{36} erg s⁻¹. Thus, the limits from *Spitzer* data alone rule out the brightest red giants, but not red giants with moderate to low luminosities.

The *Spitzer* mid-IR upper limits are potentially useful as constraints on the DD models. Shen et al. (2011)²⁴ suggests that, for a DD merger to produce a SN Ia, it needs to evolve and cool slowly, for $> 1 \times 10^6$ yr. This means the merger product would radiate at smaller than a fraction ($\sim 1\%$) of the Eddington limit ($\sim 4 \times 10^{38}$ erg s⁻¹), i.e., less than $\sim 4 \times 10^{36}$ erg s⁻¹. The nondetections in the *Spitzer* data are thus consistent with the requirement of low IR luminosity from the DD models.

References

31. Smartt, S. Limits on Ia progenitors from pre-explosion imaging: Lessons from core-collapse progenitor studies, observational signatures of type Ia supernova progenitors. [Http://www.lorentzcenter.nl/lc/web/2010/391/presentations/Smartt.ppt](http://www.lorentzcenter.nl/lc/web/2010/391/presentations/Smartt.ppt).
32. Nugent, P. E. *et al.* Young type Ia supernova PTF11kly in M101. *The Astronomer's Telegram* **3581**, 1 (2011).
33. Li, W. *et al.* Identification of the red supergiant progenitor of Supernova 2005cs: Do the progenitors of type II-P supernovae have low mass? *Astrophys. J.* **641**, 1060–1070 (2006).
34. Li, W., Nugent, P., Bloom, J. S. & Filippenko, A. V. Analysis of the archival HST images of PTF11kly in M101. *The Astronomer's Telegram* **3582**, 1 (2011).
35. Li, W., Nugent, P., Bloom, J. S., Filippenko, A. V. & Jha, S.. Further analysis of the archival HST images of PTF11kly in M101. *The Astronomer's Telegram* **3585**, 1 (2011).
36. Smartt, S. J., Fraser, M., Kotak, R., Magill, L. & Maguire, K. No progenitor detection for PTF11kly/SN2011fe in Hubble Space Telescope pre-explosion images. *The Astronomer's Telegram* **3623**, 1 (2011).
37. Sirianni, M. *et al.* The photometric performance and calibration of the Hubble Space Telescope Advanced Camera for Surveys. *Publ. Astron. Soc. Pac.* **117**, 1049–1112 (2005).
38. Holtzman, J. A. *et al.* The performance and calibration of WFPC2 on the Hubble Space Telescope. *Publ. Astron. Soc. Pac.* **107**, 156–178 (1995).
39. Holtzman, J. A. *et al.* The Photometric performance and calibration of WFPC2. *Publ. Astron. Soc. Pac.* **107**, 1065–1093 (1995).
40. Castelli, F. & Kurucz, R. L. New grids of ATLAS9 model atmospheres. *ArXiv Astrophysics e-prints* (2004). [arXiv:astro-ph/0405087](https://arxiv.org/abs/astro-ph/0405087).
41. Pickles, A. J. A stellar spectral flux library: 1150–25000 Å. *Publ. Astron. Soc. Pac.* **110**, 863–878 (1998).
42. Schlegel, D. J., Finkbeiner, D. P. & Davis, M. Maps of dust infrared emission for use in estimation of reddening and cosmic microwave background radiation foregrounds. *Astrophys. J.* **500**, 525–553 (1998).
43. Woosley, S. E. & Weaver, T. A. Sub-Chandrasekhar mass models for type Ia supernovae. *Astrophys. J.* **423**, 371–379 (1994).
44. Fink, M. *et al.* Double-detonation sub-Chandrasekhar supernovae: can minimum helium shell masses detonate the core? *Astron. Astrophys.* **514**, A53 (2010).
45. Kato, M., Hachisu, I., Kiyota, S. & Saio, H. Helium nova on a very massive white dwarf: A revised light-curve model of V445 Puppis (2000). *Astrophys. J.* **684**, 1366–1373 (2008).
46. Di Stefano, R., Voss, R. & Claeys, J. S. W. Spin-up/spin-down models for type Ia supernovae. *Astrophys. J.* **738**, L1 (2011).
47. Justham, S. Single-degenerate type Ia supernovae without hydrogen contamination. *Astrophys. J.* **730**, L34 (2011).
48. Lee, M. G., Freedman, W. L. & Madore, B. F. The tip of the red giant branch as a distance indicator for resolved galaxies. *Astrophys. J.* **417**, 553–559 (1993).
49. Salaris, M., Cassisi, S. & Weiss, A. Red giant branch stars: The theoretical framework. *Publ. Astron. Soc. Pac.* **114**, 375–402 (2002).

50. Gromadzki, M., Mikolajewska, J. & Lachowicz, P. Post-outburst variations in the optical light curve of RS Ophiuchi. In A. Evans, M. F. Bode, T. J. O'Brien, & M. J. Darnley (ed.) *RS Ophiuchi (2006) and the Recurrent Nova Phenomenon*, vol. 401 of *Astronomical Society of the Pacific Conference Series*, 219 (2008).
51. Barry, R. K. *et al.* On the distance of RS Ophiuchi. In A. Evans, M. F. Bode, T. J. O'Brien, & M. J. Darnley (ed.) *RS Ophiuchi (2006) and the Recurrent Nova Phenomenon*, vol. 401 of *Astronomical Society of the Pacific Conference Series*, 52 (2008).
52. Iijima, T. Circumstellar envelope of RS Ophiuchi. In A. Evans, M. F. Bode, T. J. O'Brien, & M. J. Darnley (ed.) *RS Ophiuchi (2006) and the Recurrent Nova Phenomenon*, vol. 401 of *Astronomical Society of the Pacific Conference Series*, 115 (2008).
53. Anupama, G. C. & Mikolajewska, J. Recurrent novae at quiescence: systems with giant secondaries. *Astron. Astrophys.* **344**, 177–187 (1999).
54. Straizys, V. & Kuriliene, G. Fundamental stellar parameters derived from the evolutionary tracks. *Astrophys. Spa. Sci.* **80**, 353–368 (1981).
55. Belczynski, K. & Mikolajewska, J. New binary parameters for the symbiotic recurrent nova T Coronae Borealis. *Mon. Not. R. Astron. Soc.* **296**, 77–84 (1998).
56. Podsiadlowski, P. On the evolution and appearance of a surviving companion after a type Ia supernova explosion. *ArXiv Astrophysics e-prints* (2003). arXiv:astro-ph/0303660.
57. Filippenko, A. V., Li, W. D., Treffers, R. R. & Modjaz, M. The Lick Observatory Supernova Search with the Katzman Automatic Imaging Telescope. In B. Paczynski, W.-P. Chen, & C. Lemme (ed.) *IAU Colloq. 183: Small Telescope Astronomy on Global Scales*, vol. 246 of *Astronomical Society of the Pacific Conference Series*, 121 (2001).
58. Cenko, S. B. *et al.* The automated Palomar 60 inch telescope. *Publ. Astron. Soc. Pac.* **118**, 1396–1406 (2006).
59. Kasliwal, M. M. *et al.* Discovery of a new photometric subclass of faint and fast classical novae. *Astrophys. J.* **735**, 94 (2011).
60. Rau, A. *et al.* Exploring the optical transient sky with the Palomar Transient Factory. *Publ. Astron. Soc. Pac.* **121**, 1334–1351 (2009).
61. Law, N. M. *et al.* The Palomar Transient Factory: System overview, performance, and first results. *Publ. Astron. Soc. Pac.* **121**, 1395–1408 (2009).
62. Benjamini, Y. & Hochberg, Y. Controlling the false discovery rate: A practical and powerful approach to multiple testing. *Journal of the Royal Statistical Society. Series B (Methodological)* **57**, 289–300 (1995).
63. Miller, C. J. *et al.* Controlling the false-discovery rate in astrophysical data analysis. *Astron. J.* **122**, 3492–3505 (2001).
64. Livio, M. Classical novae and the extragalactic distance scale. *Astrophys. J.* **393**, 516–522 (1992).
65. Cash, W. Parameter estimation in astronomy through application of the likelihood ratio. *Astrophys. J.* **228**, 939–947 (1979).
66. Kalberla, P. M. W. *et al.* The Leiden/Argentine/Bonn (LAB) survey of galactic HI. Final data release of the combined LDS and IAR surveys with improved stray-radiation corrections. *Astron. Astrophys.* **440**, 775–782 (2005).
67. Gilfanov, M. & Bogdán, Á. An upper limit on the contribution of accreting white dwarfs to the type Ia supernova rate. *Nature* **463**, 924–925 (2010).

68. Hachisu, I., Kato, M. & Nomoto, K. Supersoft x-ray phase of single degenerate type Ia supernova progenitors in early-type galaxies. *Astrophys. J.* **724**, L212–L216 (2010).
69. Ardila, D. R. *et al.* SpS1-The Spitzer atlas of stellar spectra. *Highlights of Astronomy* **15**, 512–512 (2010).